MORPHOLOGIC AND COMPUTATIONAL FLUID DYNAMIC ANALYSIS OF SAND DUNE-TOPOGRAPHIC OBSTACLE INTERACTIONS ON EARTH AND TITAN

An Undergraduate Research Scholars Thesis

by

JULIA CISNEROS

Submitted to Honors and Undergraduate Research
Texas A&M University
in partial fulfillment of the requirements for the designation as an

UNDERGRADUATE RESEARCH SCHOLAR

Approved by
Research Advisor: Dr. Ryan C. Ewing

May 2015

Major: Geology

TABLE OF CONTENTS

Page

ABSTRACT 1

DEDICATION 3

ACKNOWLEDGEMENTS 4

SECTION

I INTRODUCTION AND BACKGROUND 5

1. Introduction and Motivation 5
2. Study Area 9

II METHODS 12

3. Mapping Analysis 12
4. Computational Fluid Dynamic (CFD) Analysis 13

III RESULTS 18

5. Mapping Analysis Results 18
6. CFD Analysis Results 26

IV DISCUSSION 37

7. Earth Geomorphic Mapping Discussion 37
8. Titan Radar Unit Mapping Discussion 37
9. CFD Analysis Discussion 38

REFERENCES 40

APPENDIX A 42

ABSTRACT

Morphologic and Computational Fluid Dynamic Analysis of Sand Dune-Topographic Obstacle Interactions on Earth and Titan. (May 2015)

Julia Cisneros
Department of Geology and Geophysics
Texas A&M University

Research Advisor: Dr. Ryan C. Ewing
Department of Geology and Geophysics

Earth and Titan have vastly different physical environments, but similar landscapes. Sand dunes, like those found in Earth's deserts, cover large areas of Titan's equatorial region and are important records of climate. Titan's linear dunes and their interaction with topographic obstacles within the dune fields are thought to indicate westerly wind flow, which is opposite the easterly flow expected based on the spin of Titan and predicted from several global climate models (GCMs). The westerly interpretation of wind direction is largely based on the notion that the dunes represent streamlines that flow around the obstacles. However, the mechanics of how sand dunes are deflected around an obstacle is poorly understood. We examine the interactions between linear dunes and topographic obstacles by mapping the morphology of the obstacles and nearby dunes and using computational fluid dynamic (CFD) analysis of wind flow near obstacles. We map dune crest line orientation, obstacles, and other morphologies using visible satellite imagery for Earth and Cassini radar imagery for Titan. Obstacles length, width and height are mapped from both satellite imagery and digital terrain models (DTMs). We input obstacle topography and GCM and weather station data into WindNinja 2.2.0, a simple CFD. We use the CFD model to estimate wind velocity and direction near the obstacles, calculate gross bedform normal transport, and determine dune orientations around the obstacles. Our results

indicate greatest variations in wind velocity and direction for regions within 500 meters of the obstacle and uniform wind flow patterns outside this zone. The modeled dune orientations also deviate greatest from the mean regional orientations in the upwind side of the obstacle. Topographically, the upwind side is higher than the downwind side, which could be a topographic signature of transport direction. These observations are consistent on both Earth and Titan. Identifying how dune patterns and topographic signatures of sand transport are affected by wind interactions with obstacles on Titan provides a new basis to evaluate wind directions on Titan.

DEDICATION

I would like to dedicate this thesis to my parents who have always supported my need to ask "Why?".

ACKNOWLEDGEMENTS

My sincerest thanks to Dr. Ryan C. Ewing for his mentorship throughout this project and the numerous opportunities he has given me to become a better scientist. I would also like to thank my collaborators for their valuable feedback. This project was supported by NASA CDAP NNX14AD52G.

SECTION I

INTRODUCTION AND BACKGROUND

1. Introduction and Motivation

Linear dunes, or dunes with straight crestlines, mantle the equatorial region of Titan (Figure 1)(Lorenz et al., 2006; Radebaugh et al., 2010; Rubin and Hesp, 2009). These dunes are a primary record of the winds and sand transport at the surface of Titan and are thought to be linked to changes in Titan's climate over the past tens of thousands of years (Ewing et al., 2015). Although the dunes are generated by wind, linear sand dunes can form by different wind regimes, and thus are not diagnostic of any given wind direction. Although, barchan, star and reoriented dunes have been used to interpret wind directions, wind and sand transport direction is primarily based upon the interaction between the linear dunes and topographic obstacles, which sit among the dunes (Figure 2).

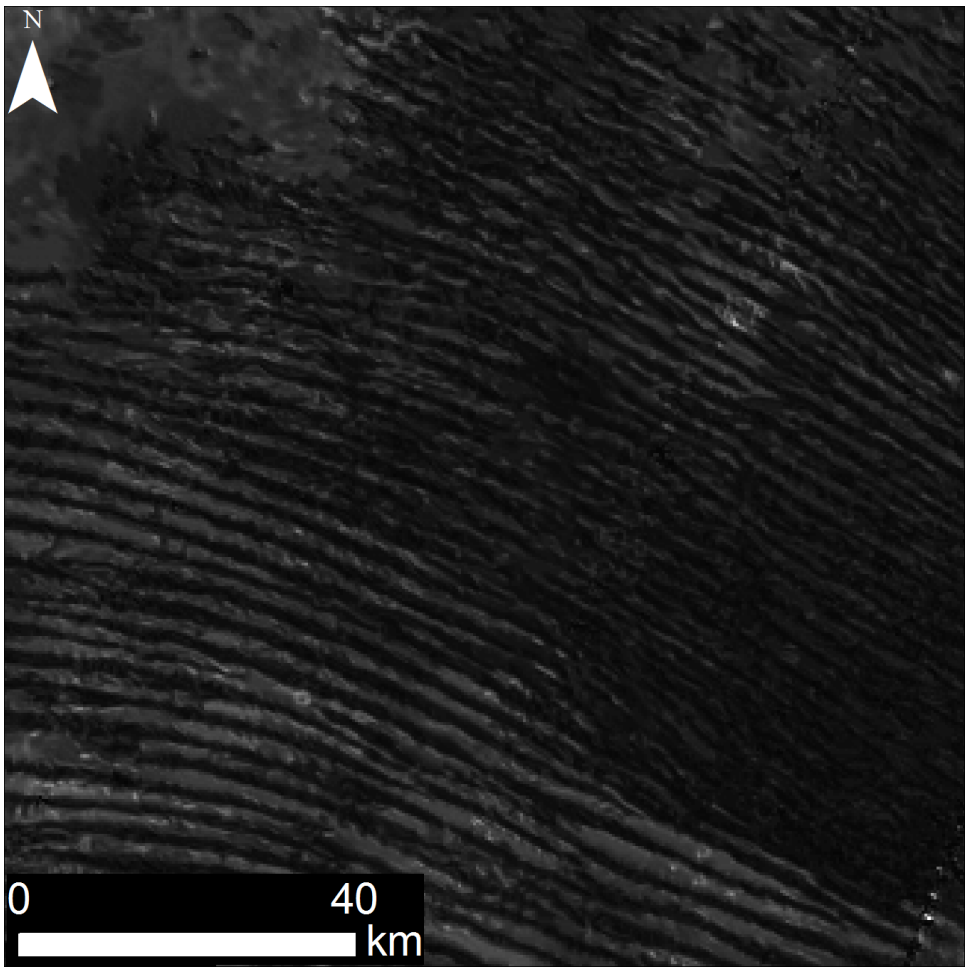

Figure 1: Linear dunes in the Shangri-La Dune Field, Titan. All images used are denoised Cassini synthetic aperture radar (SAR) data. For denoising method see Lucas et al., 2014. Radar dark areas are smooth and interpreted to be sand dunes. Radar bright areas scatter the radar and are interpreted to be interdune areas.

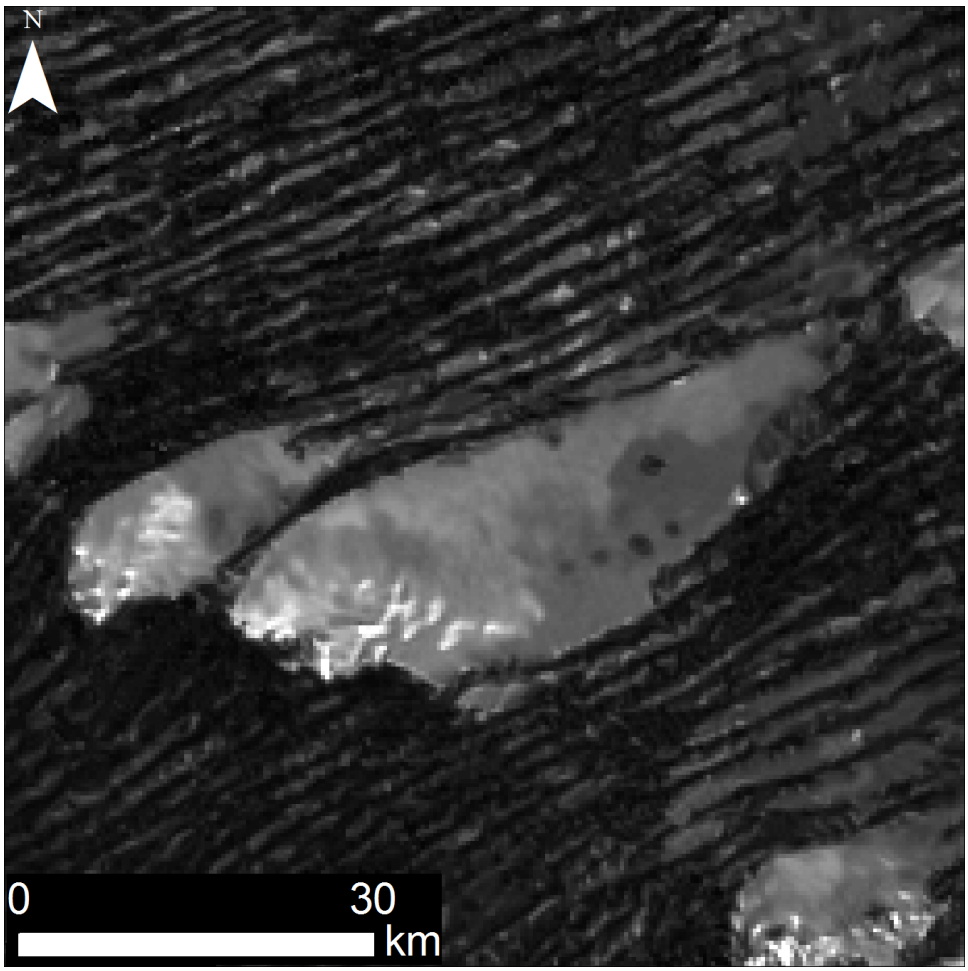

Figure 2: Linear dunes interacting with obstacle in the Belet Dune Field, Titan. Note the streamlined, teardrop appearance of the obstacle and the deflection of the dark dunes around the obstacle. This shape provides the basis for the hypothesis that the dunes are streamlines and flowing around the obstacle (Lorenz et al., 2006).

Topographic obstacles, designated by radar bright areas, are also found throughout Titan's equatorial dunes (Figure 2). The obstacles vary in size and shape and in many instances have a tear-drop like shape where one side tapers to a point. The linear dunes diverge around obstacles paralleling the tear-dropped shape of the obstacle. The interpretation that this shape indicates flow direction is based on how streamlines appear in a fluid moving around an obstacle (Figure 3). Whereas, this idea is appropriate for a fluid under unidirectional flow, is it an appropriate model for sediment transport and multimodal winds?

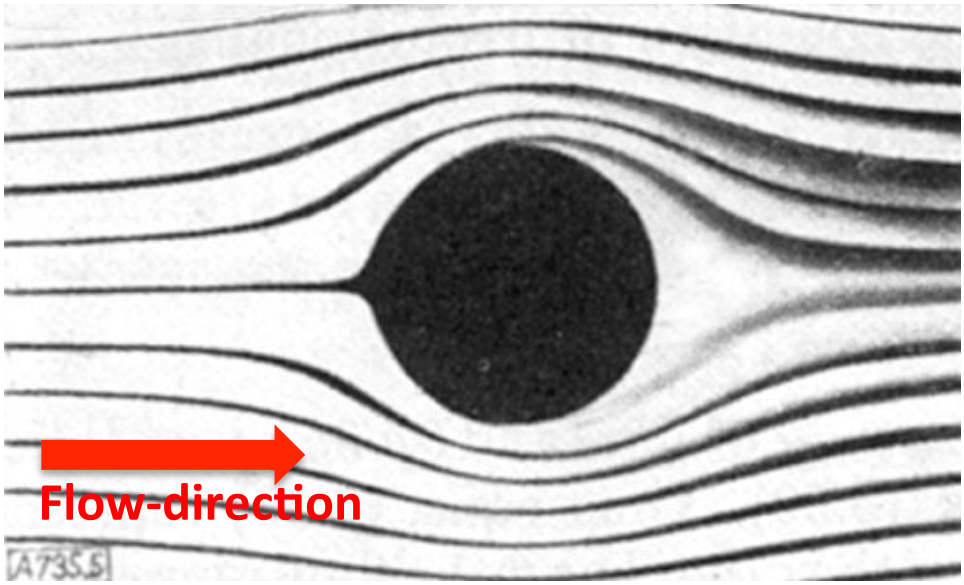

Figure 3: Streamlines in fluid flow around an obstacle. Streamlines are black streaks across the image and the obstacle is the black circle. Streamlines diverge around the obstacle and re-align in the lee side. Flow direction is from the left.

Based on the streamline model, the interaction of dunes around the obstacles on Titan led to the idea that sand transport was from west to east (Lorenz et al., 2006; Lorenz and Radebaugh, 2009; Radebaugh et al., 2010), however, interpretations of wind direction remain highly variable (Rubin and Hesp, 2009). The most widely recognized model of Titan's equatorial wind regime is based on a GCM. Tokano (2010) used a GCM to model wind directions at different wind threshold velocities and showed that westerly winds occurred at high threshold wind velocities and were predominant during seasonal changes on Titan. The overall wind regime was multimodal with a bimodal easterly wind component (Tokano, 2010). More recently Ewing et al. (2015) estimated timescales needed to reorient dunes in the equatorial region that are longer than diurnal, seasonal, or tidal winds (Ewing et al., 2015). Lucas et al. (2014) suggests that the current dune crestline orientation is consistent with strong westerly winds and sand dunes forming in an availability limited environment, similar to that suggested by Tokano (2010) (Lucas et al., 2014b).

With the motivation to determine the geomorphic signature of wind and sand transport direction from dune-topographic obstacle interactions, we analyze this interaction on both Earth and Titan. We analyze dune interactions with topography of Southern Mauritania and in the Shangri-La Dune field on Titan using geomorphic mapping and CFD analysis. The findings of this paper are (1) the complex wind flow around the obstacle creates a complex geomorphic environment around the obstacle, (2) the complexity of the wind has a strong influence on the spatial variations of sand transport and dune orientation, and (3) bimodal winds that could form linear longitudinal dunes could also transport sand into the lee side of an obstacle, which suggests the bimodal component of Titan's winds may not be the primary sand transporting wind.

2. Study Area

The study area on Earth is located in southern Mauritania in western Africa (Latitude 17.398764° decimal degrees, Longitude -11.380843° decimal degrees) (Figure 4) and part of the western Saharan desert. Geomorphically, the region is dominated by sand dunes, ephemeral rivers and rocky uplands. The study area was chosen because of the distinct, isolated topographic obstacles surrounded by dunes. Of three prominent topographic obstacles in the local area (Figure 4), we chose to focus on the southwestern most obstacle because (1) it is isolated from the other obstacles, a nearby river, and nearby plateau. (2) The obstacle creates a streamlined appearance similar to those on Titan and the teardrop tail aligns with a regional resultant wind direction from 044º. (3) Linear and transverse dunes surround this obstacle.

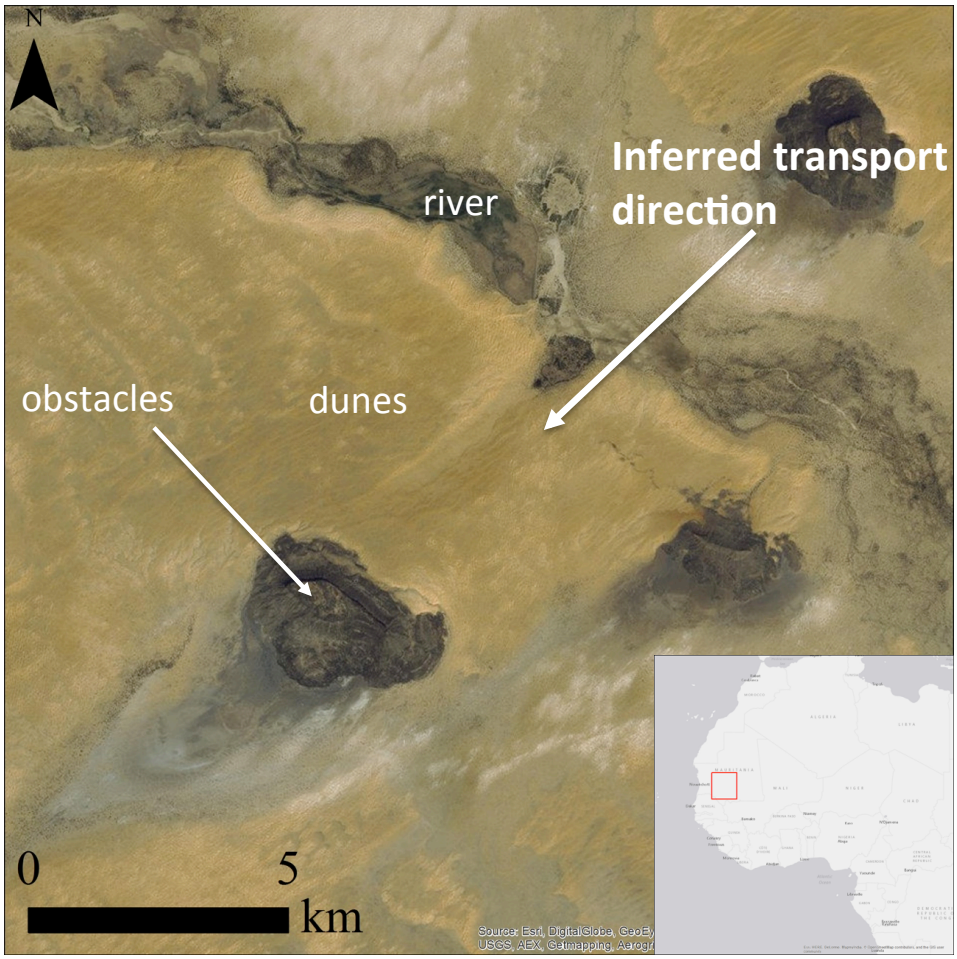

Figure 4: Study area in southern Mauritania, Africa. Visualized using an optical satellite image from Arc basemap (DigitalGlobe).

The study area for Titan is located in the Shangri-La dune field (Latitude 1.836048° decimal degrees, Longitude -150.816048° decimal degrees) (Figure 5). Observations for this area is based entirely on variations in radar brightness values where bright correspond to rough, radar reflective surface and dark correspond to smooth surface. The area has large variations in brightness, ranging from radar bright elliptical shapes, interpreted as obstacles, to radar dark lines, interpreted to be linear dunes. There are also gray areas and areas of mottled radar bright and dark spots, which may have different origins (see below). Based on GCMs, the inferred transport direction is predicted to be easterly due to the angular momentum of Titan (Tokano, 2010). We chose to focus on a particular obstacle within the dune field because (1) it is isolated

from other obstacles. (2) The obstacle depicts the streamline interaction between obstacle and dunes. (3) Synthetic aperture radar (SAR) topographic data cover half of the obstacle.

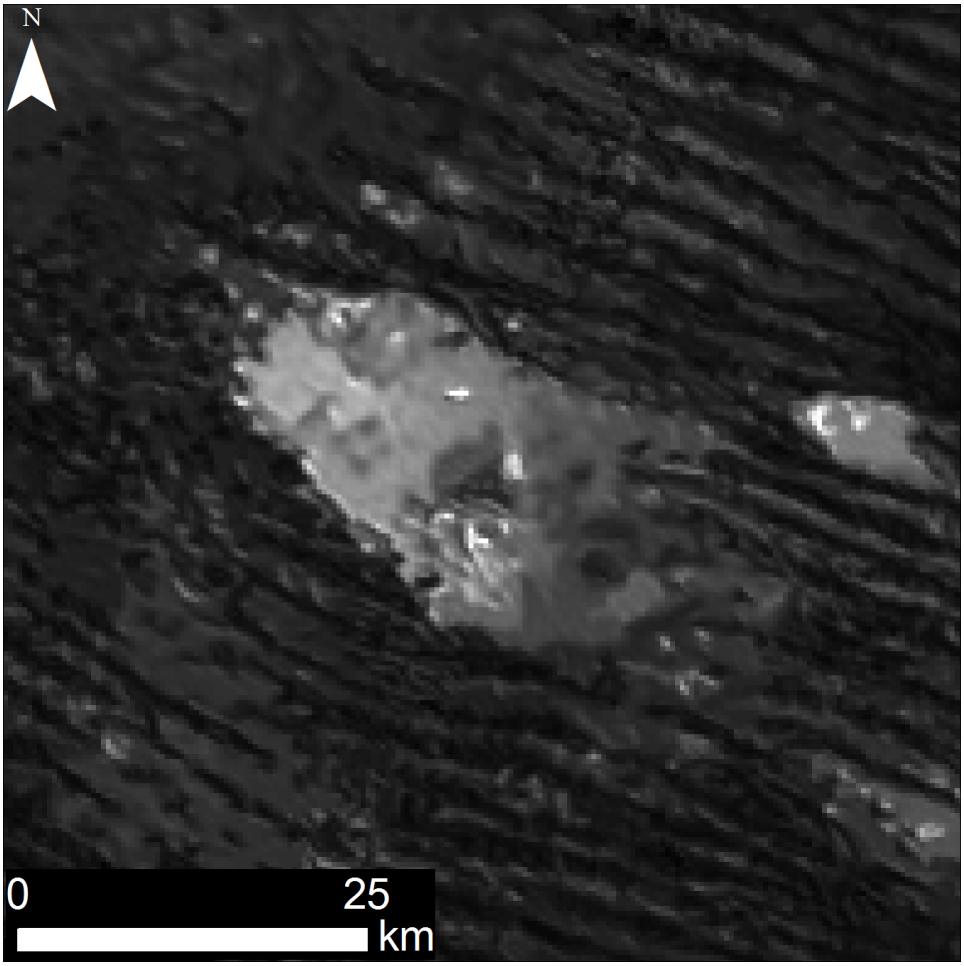

Figure 5: Study area in the Shangri-La dune field on Titan. Visualized using denoised Cassini radar imagery (Lucas et al., 2014a).

SECTION II

METHODS

3. Mapping Analysis

Dune crestlines, geomorphic units, and radar units around the obstacle were digitized using ArcGIS/ArcMap (Ewing et al., 2006) on optical satellite imagery from the Arc basemap (DigitalGlobe), Cassini SAR and digital terrain models (DTMs). The SAR data had been denoised using a non-local filtering approach (Lucas et al., 2014). This approach averages similar pixels, and it assumes there are enough redundant and noise free pixels to reduce the noise significantly. On Earth, crescentic dunes were mapped at a 1:5000 scale and superimposed linear dunes were mapped at a 1:3000 scale. Superimposed dunes were mapped away from the obstacle at a distance equal to the radius of the obstacle's major axis. All geomorphic units for Earth were mapped at 1:3000. On Titan, dune crestlines and geomorphic units were mapped at a 1:10,000 scale in the Shangri-La dune field. Because the spatial resolution of the radar is around 300 meters per pixel specific types of geomorphic features could not be identified and we used radar brightness, which is a proxy for surface roughness to map this area. Bright radar indicates scattering of the radar at the radar Ku-band wavelength – 2.17 cm. Geomorphically, this could be surface lag, crusting, evaporites or bedrock (Ewing et al., 2015). Radar smooth areas are interpreted to be sand.

Elevation profiles were measured along the long axis of each obstacle from the actual or inferred upwind side to the end of the tail on the downwind side. Elevation data was derived from ASTER datasets on Earth and Cassini SAR topographic data swaths on Titan. The Cassini SAR

topographic swaths only covered half of the Titan obstacle, so elevation data was interpolated using a nearest neighbor approach in ArcGIS given the elevation data from the profile lines across the obstacle. Obstacle profile lines on Titan were derived from the raw SAR topographic data swath boundaries.

4. Computational Fluid Dynamic (CFD) Analysis

WindNinja is a simple model that incorporates conservation of mass when modeling wind flow around an obstacle (Forthofer, 2007). It is a free program that is less computationally intensive than models that incorporate conservation of momentum. Because WindNinja does not incorporate conservation of momentum, it is does not resolve obstacle modified flows away from the obstacle surface, which limits it usefulness for interpreting dune patterns generated by secondary flows. Despite this limitation, the computationally less intensive WindNinja allowed the analysis of a full distribution of winds from weather data and from GCMs.

In order to perform the analysis using WindNinja (Figure 6), two inputs are needed: wind data and digital elevation data. Wind data was acquired from Earth weather stations for Mauritania no more than 100 km away from the obstacle and the Titan Tokano 2010 GCM (Tokano, 2010) for the Shangri-La Dune Field. Earth winds were filtered by inferred saltation threshold and chose one wind direction per day, and, similarly, Titan's winds were filtered by threshold. The digital elevation data is acquired from ASTER data sets on Earth and interpolated topographic SAR data sets from Titan.

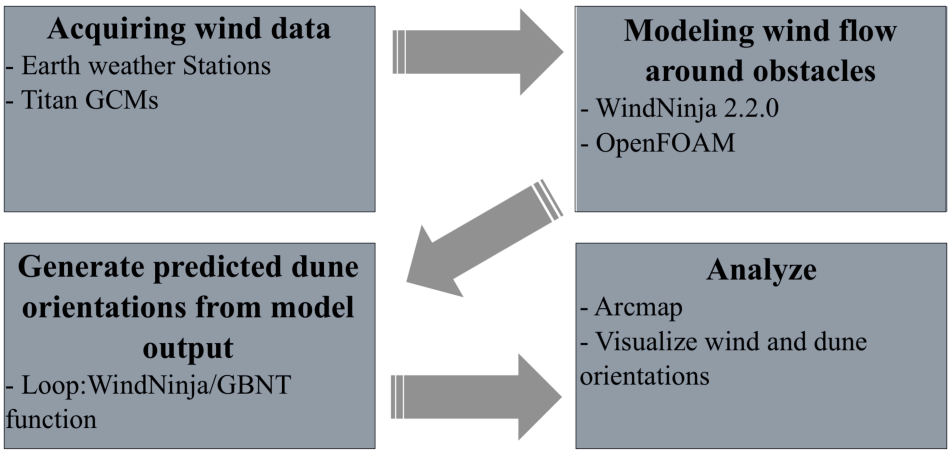

Figure 6: Flow chart of CFD analysis methods.

With this data, each filtered wind is run through WindNinja on a loop using a Matlab script (Appendix A). After getting the modified wind data for each wind, the script compiles them in a 3D matrix with x and y as ground location and z as time. The final step of the script is to use a gross bedform normal transport function (GBNT) to calculate a predicted dune orientation at each spatial point from the compiled modified winds. The GBNT function calculates the dune orientation that maximizes sand transport normal to the crestline for a given wind regime (Rubin and Hunter, 1987). The final output of this function is a spatial data matrix of dune orientation that can be overlain on the study area and visualized in ArcMap as a shape file.

The other CFD used was OpenFOAM, which is a free, open source CFD package that allows users to solve complex fluid flows. This model incorporates conservation of mass and momentum. Because it is an open source package, it can be customized. The analysis was done by collaborator Thomas Smyth from Flinders University who used a two-equation Re-normalized Group (RNG) k-epsilon airflow turbulence scheme (Smyth et al., 2012). This scheme is good for modeling secondary flows over complex terrain and accurately calculates zones of recirculation. The OpenFOAM analysis is similar to WindNinja in that it needs input winds and

digital elevation data. One wind was analyzed through OpenFOAM at a time for computational efficiency.

For the OpenFOAM analysis, scenario winds were chosen based on the wind distribution in the Earth study area (Figure 7). Winds were chosen for three scenarios: a unimodal wind from 044º, two winds, from 060º and 120º, with an acute divergence angle, and two winds, from 120º and 345º, with an obtuse divergence angle. These winds were chosen because the wind directions were all present in the wind distribution. After identifying the four winds to test, modified winds were modeled for each scenario in OpenFOAM. With the modeled wind velocities, mass flux was estimated for each wind and summed for the winds in each scenario (Eastwood et al., 2012; Tokano, 2010).

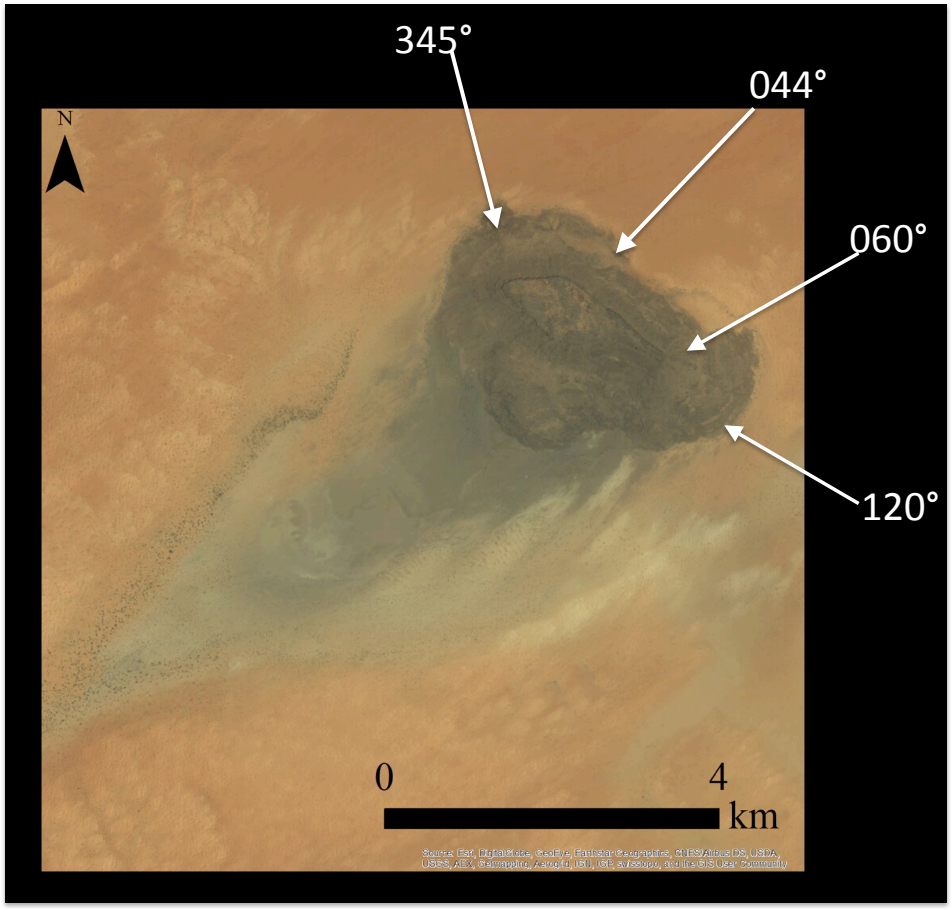

Figure 7: Wind scenarios chosen for the OpenFOAM analysis. Unimodal - 044°; Acute - 060° and 120°; Obtuse - 120° and 345°.

In order to determine areas with maximum sand flux, wind flux was estimated based on the wind velocity data. We used the approach of Eastwood et al., 2012 and Tokano 2010. The law-of-the-wall was used to calculate shear velocity, or u_*, using given variables where u_z is the wind speed at height z, κ is the von Kármán's constant (equal to 0.407 in neutral atmospheric conditions), and z_0, the height where zero velocity occurs.

$$u_z = \frac{u_*}{\kappa} \ln\left(\frac{z}{z_0}\right)$$

Then u_{*c}, the critical shear velocity to initiate movement was calculated. Where $s = \frac{\rho_s}{\rho_f}$, is the

relative density where ρ_s is sediment density and ρ_f is fluid density, g is the gravitational constant, and d is the grain diameter.

$$u_{*c} = \sqrt{0.0123(sgd + \frac{3 \times 10^{-4} {}^{kg}/_{s^2}}{\rho_f d})}$$

From this, volume flux of sediment was converted to Q_s, the mass flux of sediment.

$$Q_s = 2.61 \frac{\rho_f u_*^3}{g}(1 - \frac{u_{*c}}{u_*})(1 + \frac{u_{*c}}{u_*})^2$$

Finally, fluxes were summed from the different directions to show areas with the highest predicted sand movement.

After analyzing each scenario, the four scenario winds were run through the GBNT function to predict dune orientation. This was done because these winds were inferred to have the most dominant winds and therefore would have the largest effect on dune orientation. After getting the dune orientation output from the GBNT function, an error analysis was performed in which the mapped dune orientations were subtracted from the predicted orientations.

SECTION III

RESULTS

5. Mapping Analysis Results

5.1 Earth Geomorphic Mapping Results

The geomorphic units identified in the Earth example include a topographic obstacle, alluvial fans, drainage, an availability-limited lee-side basin, sparse vegetation-nebkha dunes, dense vegetation-nebkha dunes, and sand sheets (Figure 8). Outboard from the obstacle, complex crescent dunes trend NW-SE, whereas smaller, superimposed linear dunes trend parallel to the obstacle tail. Alluvial fans are present on the southern half of the obstacle and produce a small drainage along the edge of the obstacle. This drainage empties out into a basin southwest and downwind of the obstacle. Varying degrees of vegetation are present in the sand dune covered area. These areas vary by proximity to the leeward basin and are defined by their degree of vegetation as sparse and dense

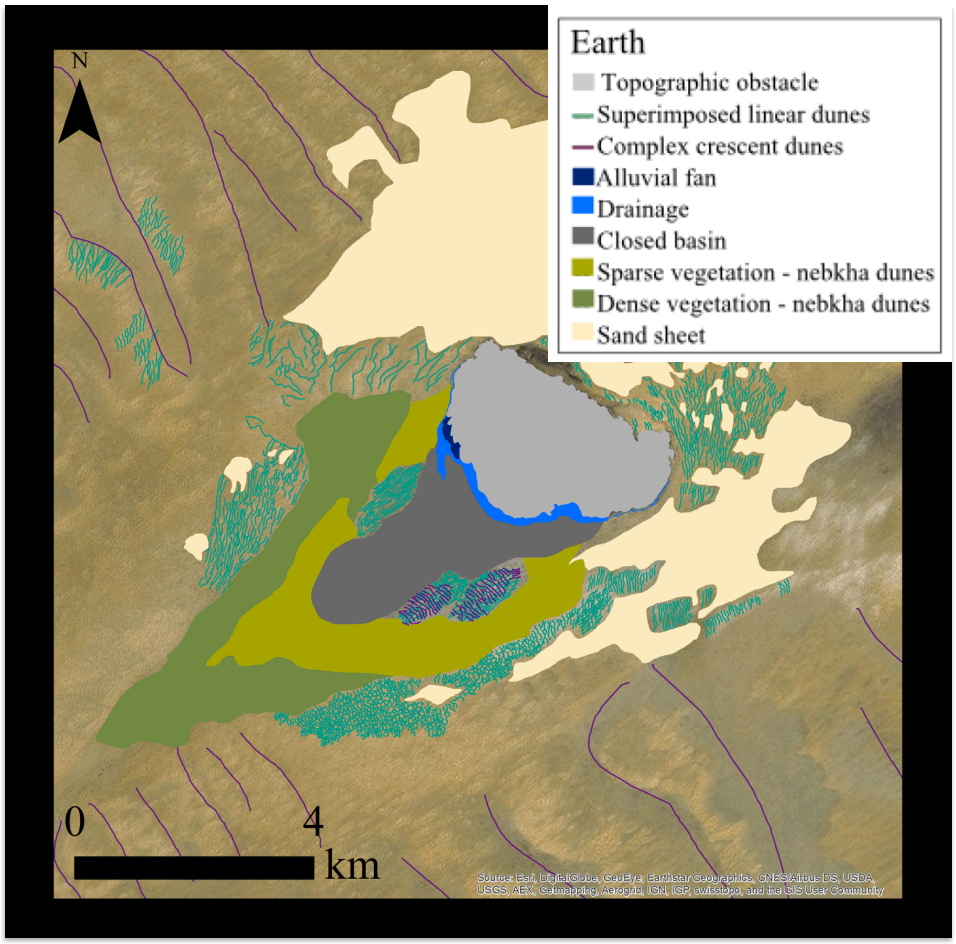

Figure 8: Geomorphic map of the Earth obstacle example.

5.1.1 Obstacle

The obstacle's height is 500 m at its peak, which is a flat plateau. The obstacle base is shaped as an ellipse with a semi major axis of 4,000 m and a semi minor axis of 2,500 m. The minor axis is approximately parallel to the resultant wind and trends NE-SW. The obstacle's average slope from base to the plateau top is 30º.

5.1.2 Availability-limited lee-side basin

The availability-limited lee-side basin is formed in the lee of the obstacle. It is adjacent to the drainage from the alluvial fans and is defined by an abrupt decrease in slope. No vegetation is

visible in this region at the spatial resolution of the imagery. The boundary of this area is defined by a change in color from dark grey within the basin to light grey or sandy brown on all sides other than the obstacle. There are also no sand dunes or other geomorphic structures visible in this area. Topographically, the area is depressed from the surrounding topography (Figure 9).

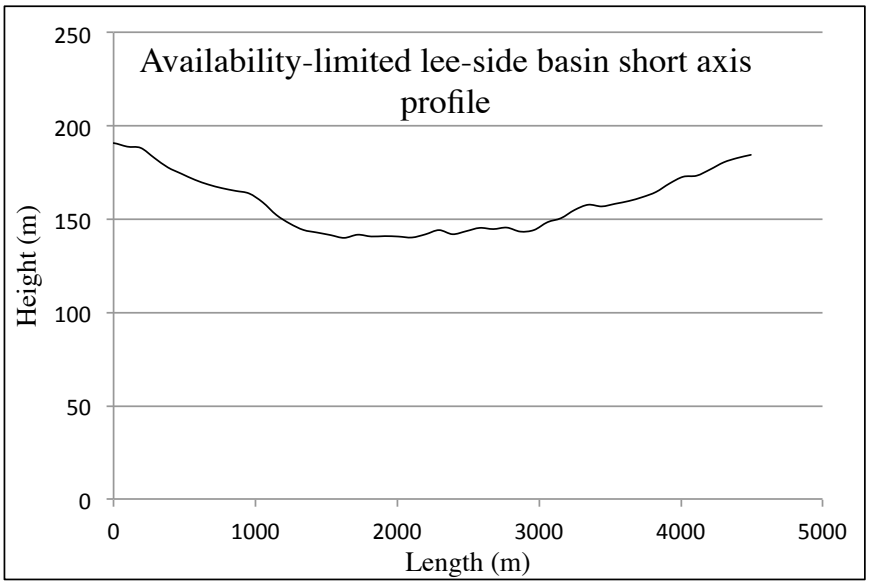

Figure 9: A topographic profile line taken along the short axis of the availability-limited lee-side basin. This profile shows the area is depressed from the surrounding topography. Topographic data is from an ASTER DTMs dataset.

5.1.3 Complex crescent dunes

The largest dunes in the study area are oriented perpendicular to the obstacle and located away from the obstacle. The dunes are spaced 1500 m and they are 5000 m long. The dunes extend across the area on either side of the obstacle but disappear close to the obstacle. Smaller linear dunes are superimposed on top of these dunes.

5.1.4 Superimposed linear dunes

The superimposed linear dunes are located in various regions around the obstacle. Some dunes are directly adjacent to the obstacle while others are adjacent to the availability-limited lee-side

basin. The dunes directly adjacent to the obstacle are deflected around the obstacle, but dune deflection does not occur more than 500 m away from the obstacle. Dunes adjacent to the availability-limited lee-side basin are not deflected, but rather align with the resultant transport.

5.1.5 Alluvial fans

Alluvial fans are present on the southwestern side of the obstacle. They exist where the obstacle's slope is less than 5º. The fans are small scale compared to the obstacle and are grouped together in a bajada, which is a cluster of alluvial fans. The fans empty at the bottom of the obstacle and create a drainage along the bottom half of the obstacle.

5.1.6 Drainage

The drainage runs along the southern half of the obstacle at the boundary between the obstacle and the availability-limited lee-side basin. This drainage exists where the slope of the obstacle is close to 0º. The mouth begins at the alluvial fans on the obstacle's western side and extends to the bottom half of eastern side. Interestingly, the drainage extends into the area of the availability-limited lee-side basin close to the alluvial fans, or where the drainage begins.

5.2 Titan Radar Unit Mapping Results

For Titan, our results are based on variations in brightness values, a proxy for surface roughness, which results in different radar units (Figure 10). The distinct radar units on Titan include a elliptical shaped radar bright unit, radar dark streaks across the area and diverging around the elliptical bright unit, a mottled radar dark and bright area adjacent to the radar bright elliptical shape, and moderate brightness areas between and crossing over the dark streaks.

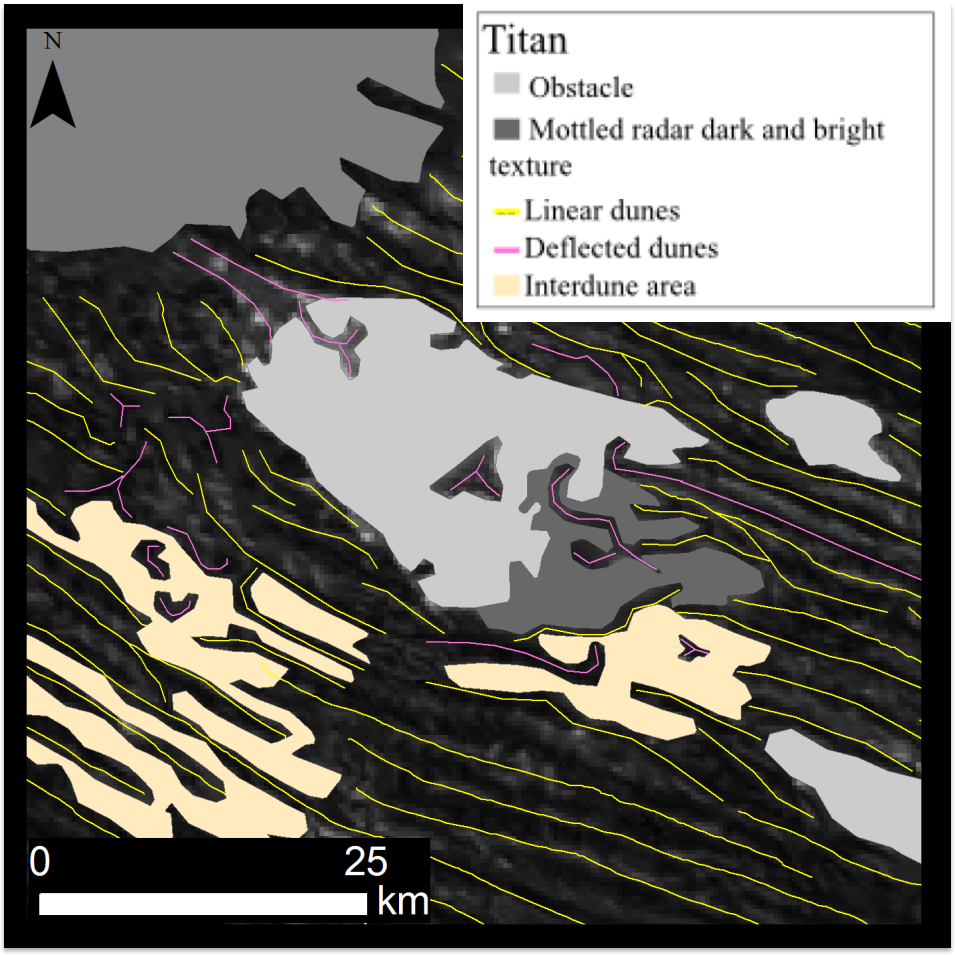

Figure 10: Geomorphic map of the Titan obstacle example.

5.2.1 Obstacle

The obstacle is categorized by having the highest brightness value (Lorenz et al., 2006; Radebaugh et al., 2010). The brightness value of this area is significantly brighter than the dark areas surrounding it, so the boundary can be clearly mapped. In some areas around the obstacle, the obstacle boundary cuts into the obstacle, disrupting the idealized smooth lined boundary. The obstacle is higher than the surrounding area, based on SAR topographic data, and the base is shaped as an ellipse, with the major axis aligned NW-SE.

5.2.2 Linear dunes

The linear dunes in this area correspond to the radar dark streaks. These dunes have straight crestlines and extend parallel to the major axis of the obstacle. The dunes diverge around the topographic obstacles and realign on the lee side of the obstacle. Further from the obstacle, the dunes are evenly spaced and do not diverge. Overall, the linear dunes here are not separated into smaller groups and they all have similar dune orientations.

5.2.3 Deflected dunes

The deflected dunes in this area are located very close to or encroach upon the obstacle. They are described as dunes that are straight crestlines that at some point curve. They can be seen extending in three directions from a midpoint, curving at the end of a linear dune, or a linear dune splitting into two legs and curving. The dunes do not exist further away from the obstacle, and leads to the assumption that like the dunes on Earth, deflection does not happen far away from the obstacle.

5.2.4 Obstacle Adjacent Radar Mottled sheet

This area is the mottled radar dark and bright area. It is directly adjacent to the obstacle in the inferred lee side. The sheet includes deflected dunes within it and linear dunes stop at its boundary. The boundary of the sheet is defined by a light grey mottled texture different from the black and white transitioning dune field and the bright white obstacle.

5.2.5 Interdune areas

Interdune areas are located between the linear dunes and are defined by a consistent moderate brightness. The boundary of these sheets is seen by the change from moderate brightness to radar dark areas. These sheets wrap around and across linear dunes and congregate. Linear dunes also stop at the sheet boundaries and deflected dunes are found within the sheets also. These sheets are only found in the southwestern side of this obstacle.

5.3 Topographic Analysis Results

From the topographic profiles taken on Earth and Titan, there is a consistent pattern. In each profile from Earth and Titan obstacles, the upwind side was higher than the downwind side (Figure 11). Initially, topographic profiles were taken from the three Earth obstacles in the Mauritania study area. The topographic profiles demonstrate that although the obstacles are different sizes, the upwind side is always higher than the downwind side. This observation is consistent with three obstacles mentioned by Radebaugh et al., 2010, one from Libya and two from Namib. These topographic profiles also showed the same signature – the upwind side was higher than the downwind side. Finally, a profile was taken from the Titan obstacle, along the long axis and through the raw SAR topographic data swath. From this topographic profile, based on relative height, the upwind side is also higher than the downwind side.

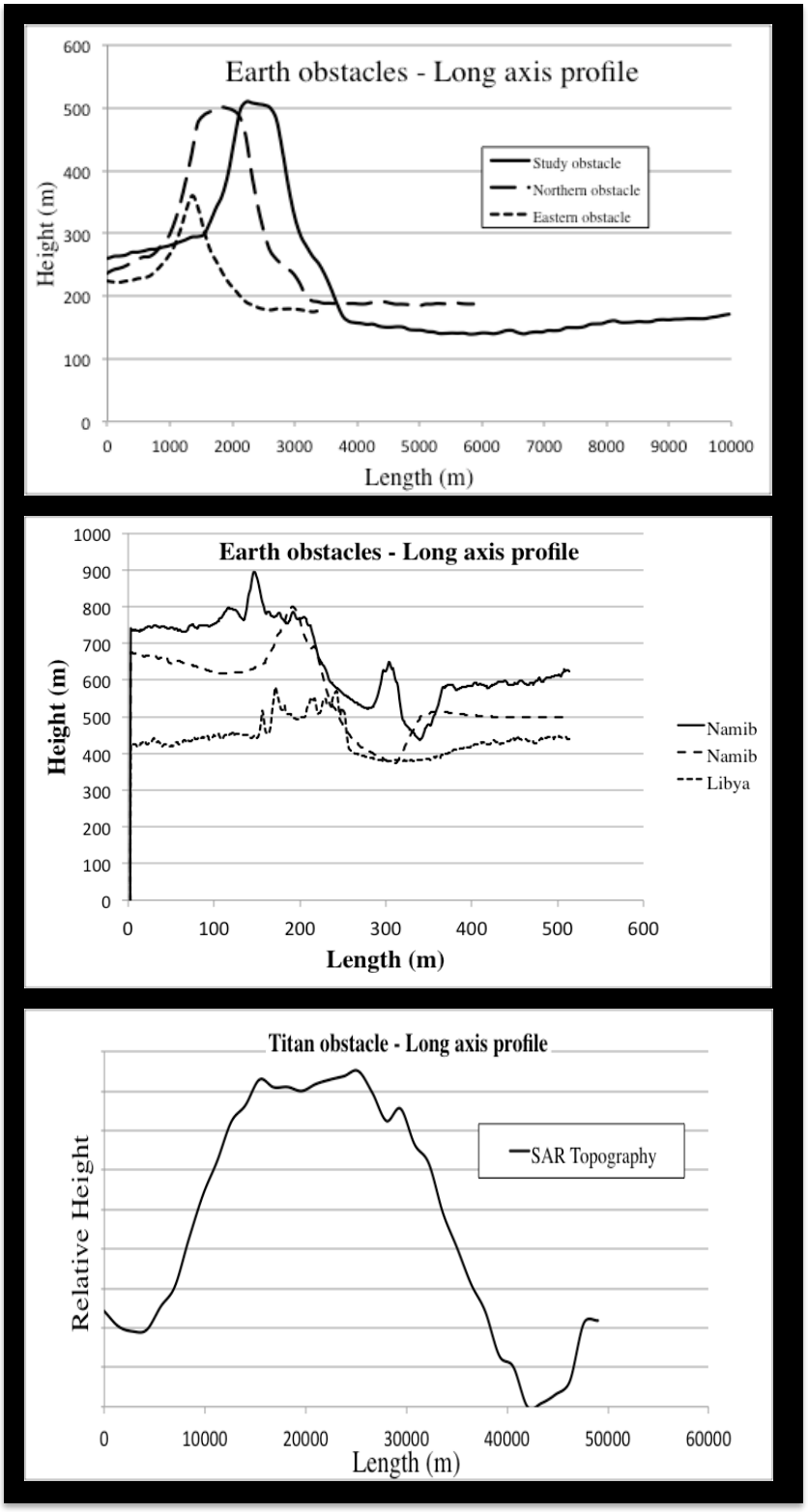

Figure 11: Topographic profiles for Earth and Titan obstacles taken from the upwind side to the downwind side in the direction of transport for the Earth examples or inferred transport direction on Titan.

6. CFD Analysis Results

WindNinja analysis for Earth show differences in wind velocity and predicted dune orientation occur between the upwind and downwind areas of the obstacle (Figure 12). A low velocity zone exists at the base of the obstacle where the wind initially contacts the obstacle on the upwind side and also in the lee side of the obstacle. The low velocity zone determined by Wind Ninja occurs only very close to the obstacle base and does not extend away from the obstacle. This is an artifact of the model and contrasts with the more sophisticated OpenFOAM model discussed later. High velocity zones in this analysis exist at the peak of the obstacle and arise because of the conservation of mass -- the flow is compressed as the height and slope of the obstacle increase. Dune orientations based upon the WindNinja modeled wind directions do not match the mapped superimposed linear dunes in the downwind area (Figure 13a). Adjacent to the obstacle, the mapped superimposed linear dunes diverge radially outward on the upwind side and do not match with the winds, but the dunes align with the predicted dunes about 500 m away from the obstacle (Figure 13c). In this region, the dunes are apparently feeling the regional wind flow and not the obstacle modified flow.

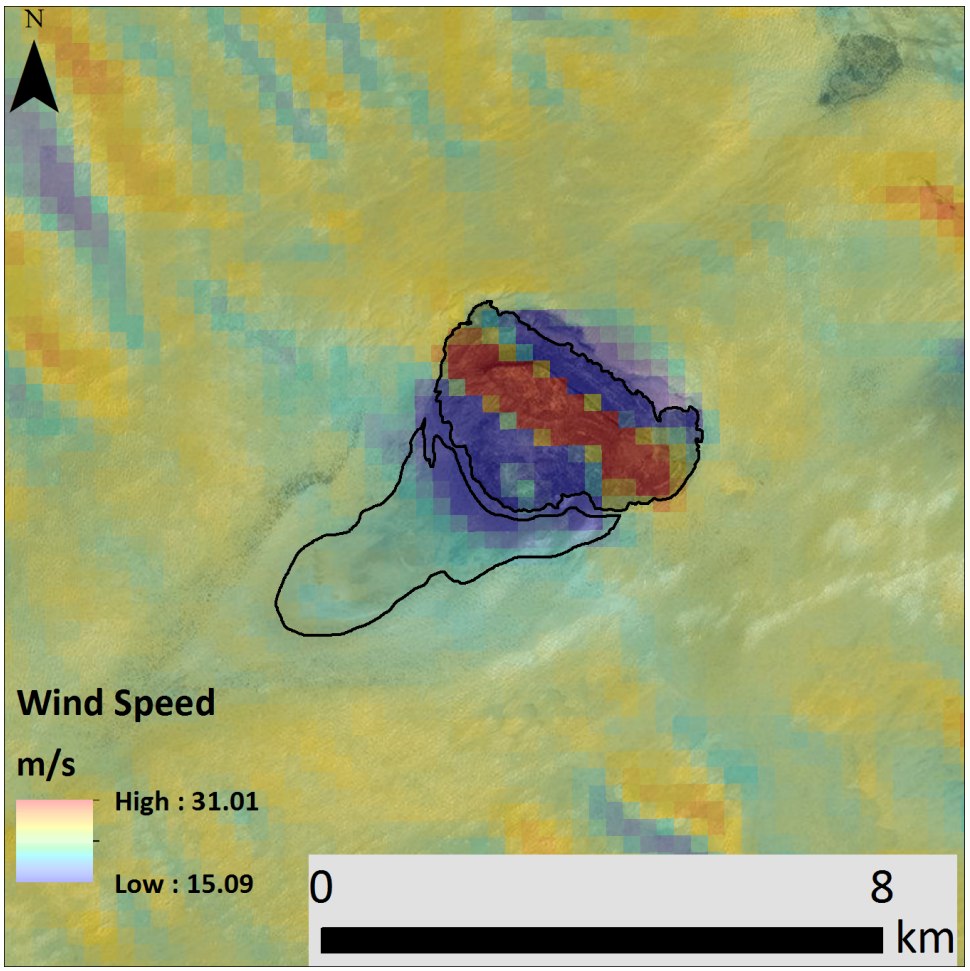

Figure 12: Wind velocity modeled by WindNinja around the Earth obstacle. Red corresponds to high velocity and blue corresponds to low velocity. Obstacle and availability-limited lee-side basin are outlined in black.

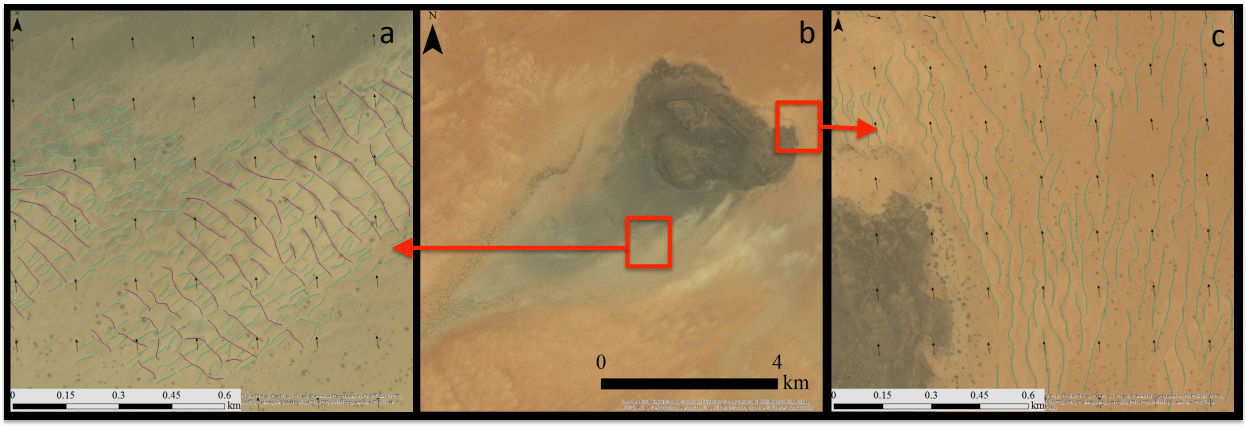

Figure 13: Comparison of predicted dunes (black arrows) from WindNinja and GBNT analysis and the mapped dunes on the upwind and downwind sides of the obstacle. In this image, (b) is the obstacle, (a) is the downwind side, and (c) is the upwind side.

On Titan, the range in GCM modeled wind velocities through WindNinja for the small area

analyzed is low – about .4 m/s (Figure 14). This is likely because the grid resolution of the model is much greater than the relatively small area analyzed. Both the obstacle modified dunes and the regional dune trend do not match the predicted dune orientations (Figure 15). Although the same upwind and downwind low velocity zones are apparent at the obstacle's base in the Wind Ninja analysis, the degree of change between the low and high velocity is not as significant as for the Earth example. This may arise because the topography on Titan is poorly constrained or the shape of the obstacle is different. Furthermore, the generalization of the Tokano 2010 GCM (Tokano, 2010) for our study area only supplies WindNinja with wind data for the whole Shangri-La sea and does not give local information. Lastly, further processing of the topographic information on the SAR topographic data swath is needed to effectively use these data in Wind Ninja.

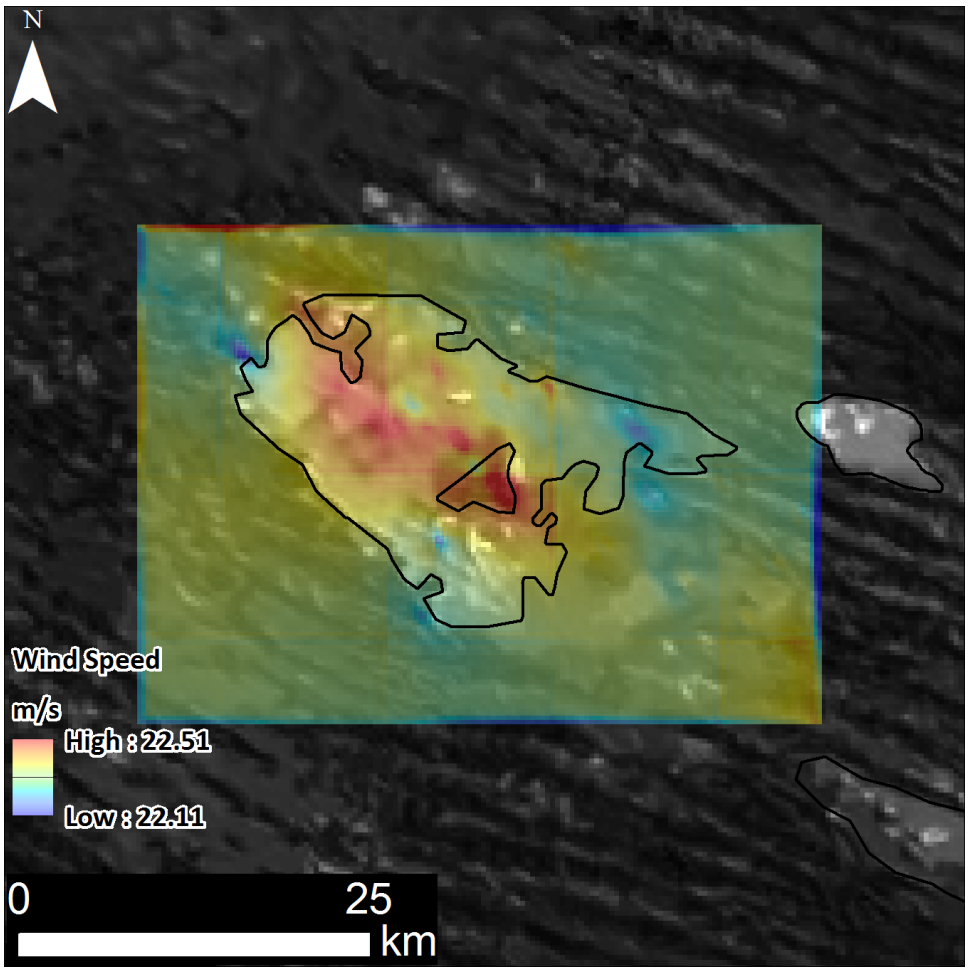

Figure 14: Wind velocity modeled by WindNinja around the Titan obstacle. Red corresponds to high velocity and blue corresponds to low velocity. The radar bright area is outlined in black.

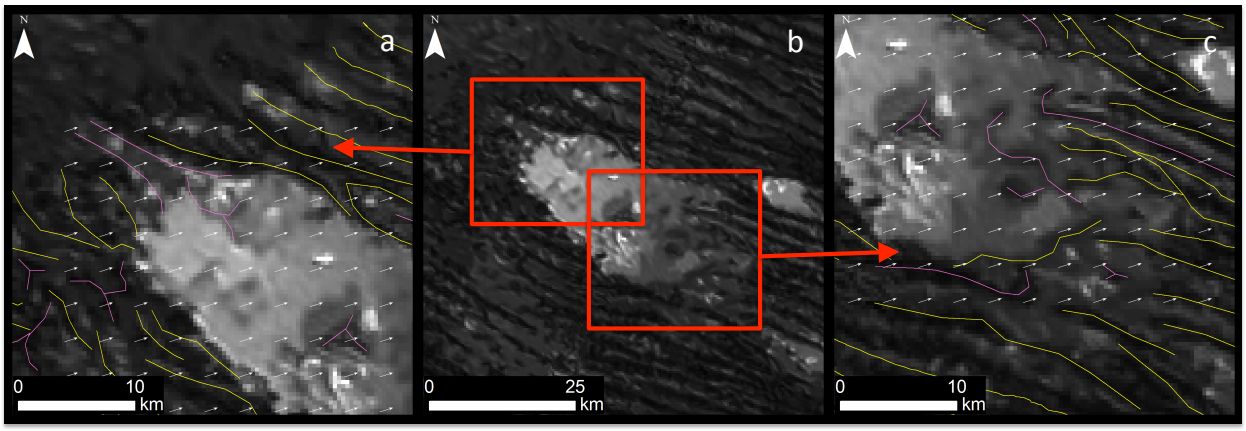

Figure 15: Comparison of predicted dunes (white arrows) from WindNinja and GBNT analysis and the mapped dunes on the upwind and downwind sides of the obstacle. In this image, (b) is the obstacle, (a) is the upwind side, and (c) is the downwind side.

In addition to the WindNinja analysis, a computational fluid dynamic analysis on the Earth study

area was performed with OpenFOAM. A unimodal wind from 044º was modeled, which is the same used for WindNinja, and considerable differences arose between the models. Much of the difference occurs on the downwind side of the obstacle where the turbulent wake would be expected, but was not captured by WindNinja. The OpenFOAM analysis shows extended low velocity zones through the tail and better matches our idea of flow interaction behind an obstacle (Figure 16). In addition, the interaction on the upwind side of the obstacle is less pronounced with the addition of the conservation of momentum. OpenFOAM captured the secondary flow and the low velocity wake on the lee side of the obstacle. Interestingly, the low velocity wake of the obstacle is offset from the sediment availability tail of the obstacle where the full wind distribution is considered.

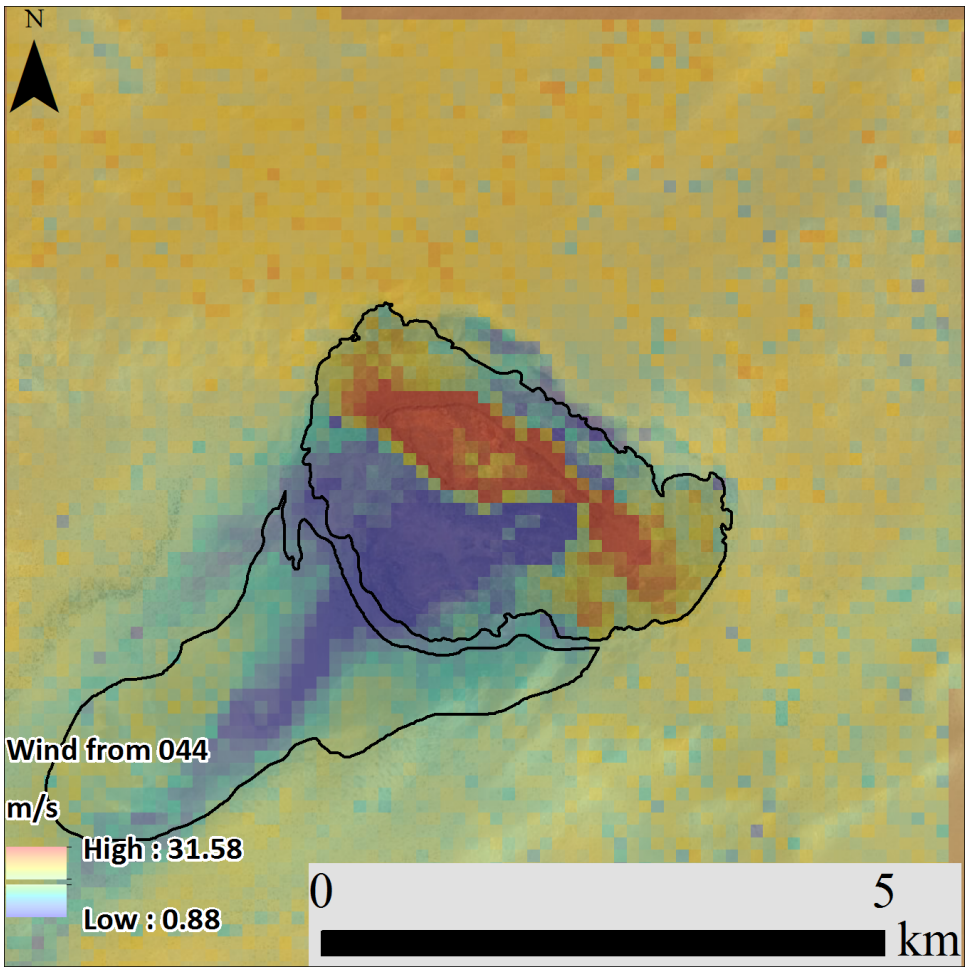

Figure 16: Modeled wind velocity around the Earth obstacle using OpenFOAM. Red corresponds to high velocity and blue corresponds to low velocity.

Results from OpenFOAM show low velocities when flow meets the base of the obstacle, higher velocity towards the top of the obstacle as flow is compressed and accelerated (Figure 17). A low velocity wake then extends through the lee of the obstacle. The wind from 044º shows a low velocity wake through the lee of the obstacle, but the wake is offset from the tail of the obstacle (Figure 17a). Modeled winds from 060º are only slightly different from a wind from 044º and show a different lee wake (Figure 17b). Moreover, looking at winds from 120º and 345º, the low velocity zones do not line up with the tail of the obstacle at all (Figure 17 c, d). The low velocity wake of 120º extends northwest (Figure 17 c) and the low velocity wake of 345º extends southeast (Figure 17 d) as expected, but the same low velocity zone still exists when flow meets

the base of the obstacle and a higher velocity occurs as flow climbs towards the top of the obstacle.

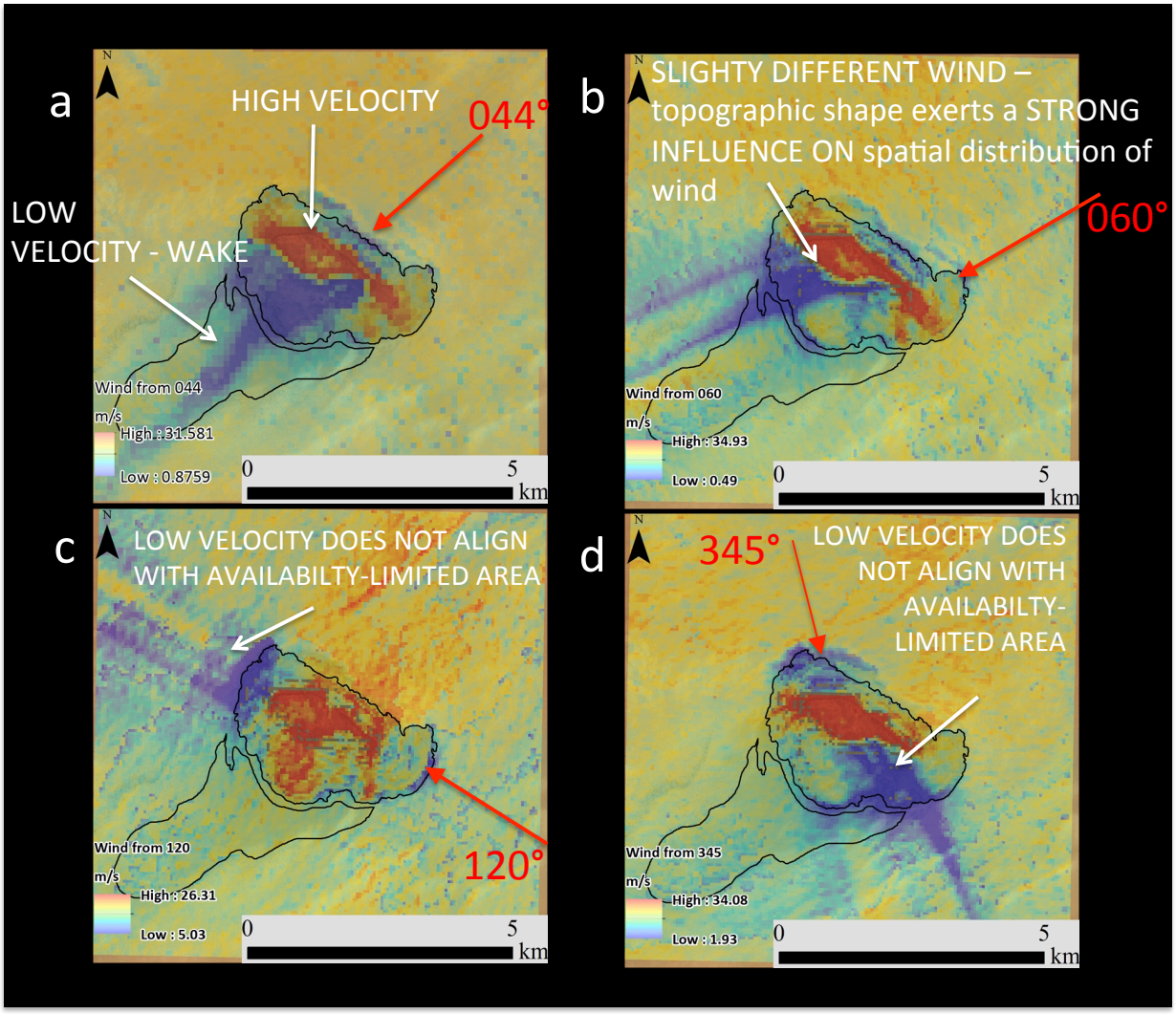

Figure 17: Modeled wind velocities for all scenarios using OpenFOAM.

In addition to the velocities, sediment flux was calculated and summed from each scenario in order see where transport was maximized around the obstacle. Unimodal and acute wind scenarios show low flux in the lee of the obstacle, which is consistent in areas with the low-velocity zone (Figure 18, 19). Interestingly, this is not seen for an obtuse wind. For the summation of flux for the obtuse winds, one from 120º and another from 345º, low flux is

observed along the sides of the obstacle (Figure 20). Contrary to the unimodal and acute winds, moderate to high fluxes are in the lee of the obstacle.

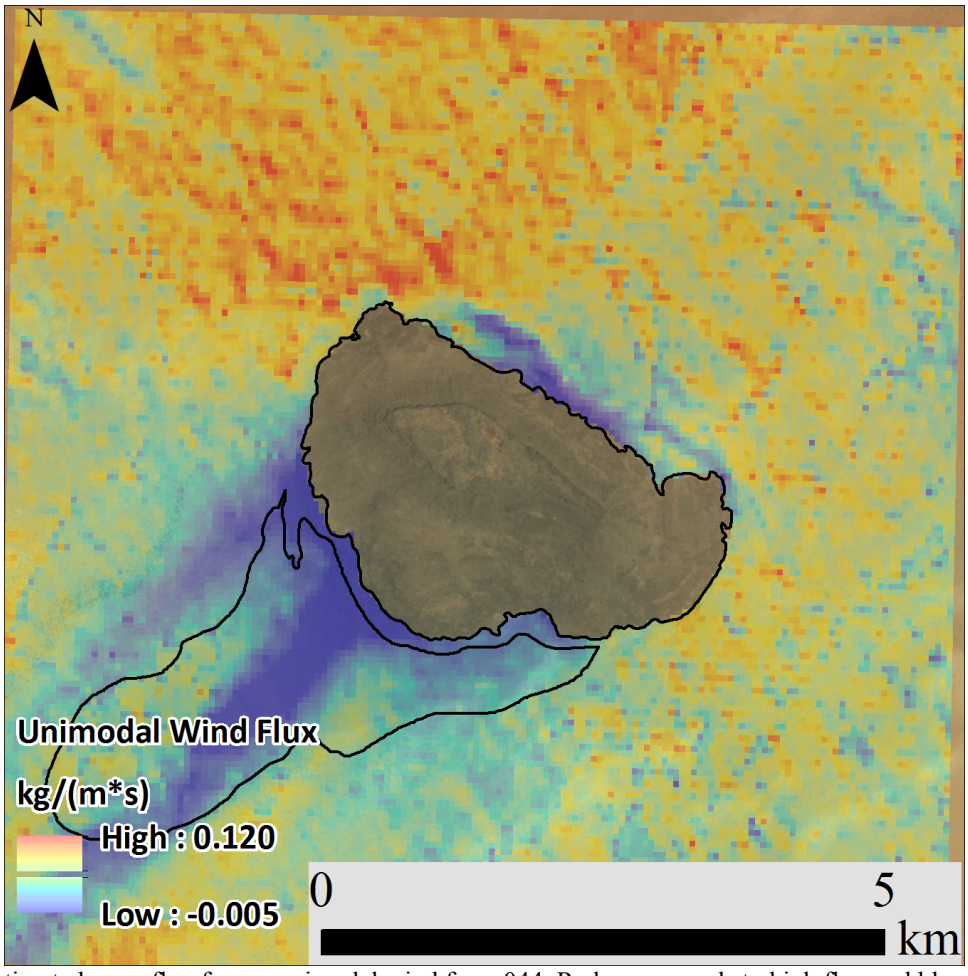

Figure 18: Estimated mass flux from a unimodal wind from 044. Red corresponds to high flux and blue corresponds to low flux. The obstacle and lee-side basin are outlined in black.

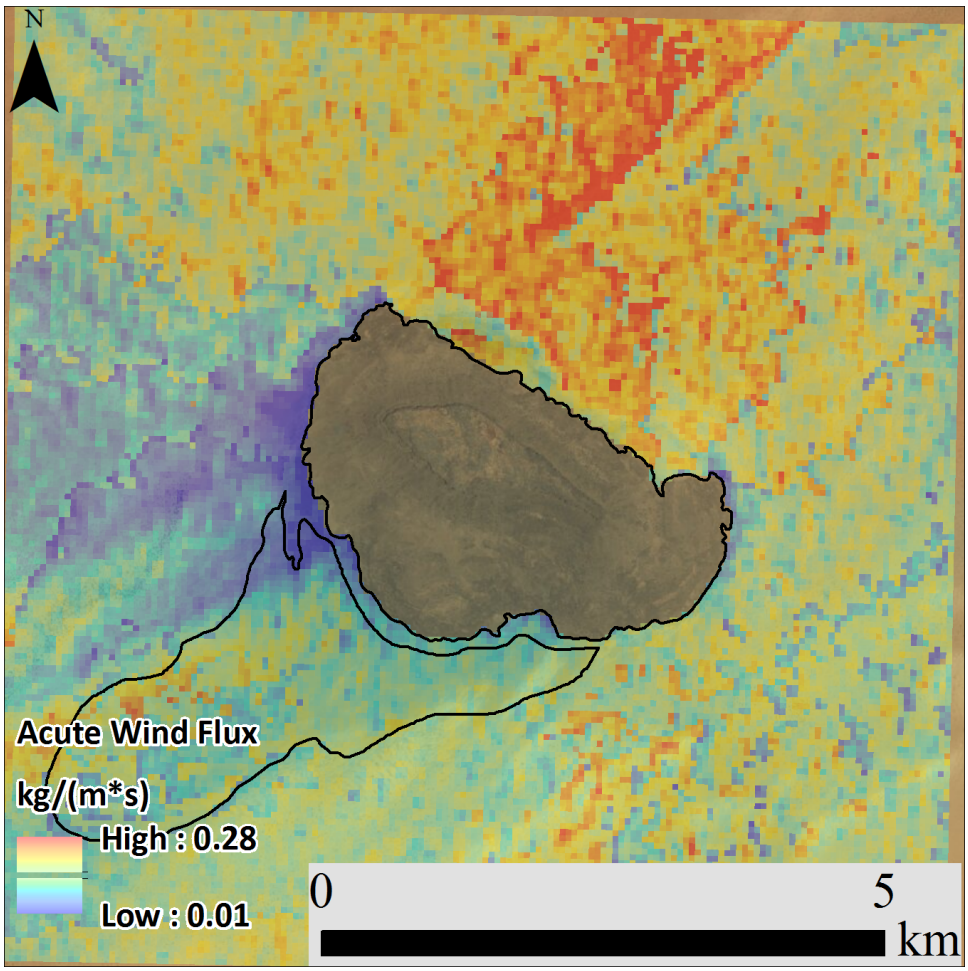

Figure 19: Estimated mass flux from an acute wind scenario - winds from 060º and 120º. Red corresponds to high flux and blue corresponds to low flux. The obstacle and lee-side basin are outlined in black.

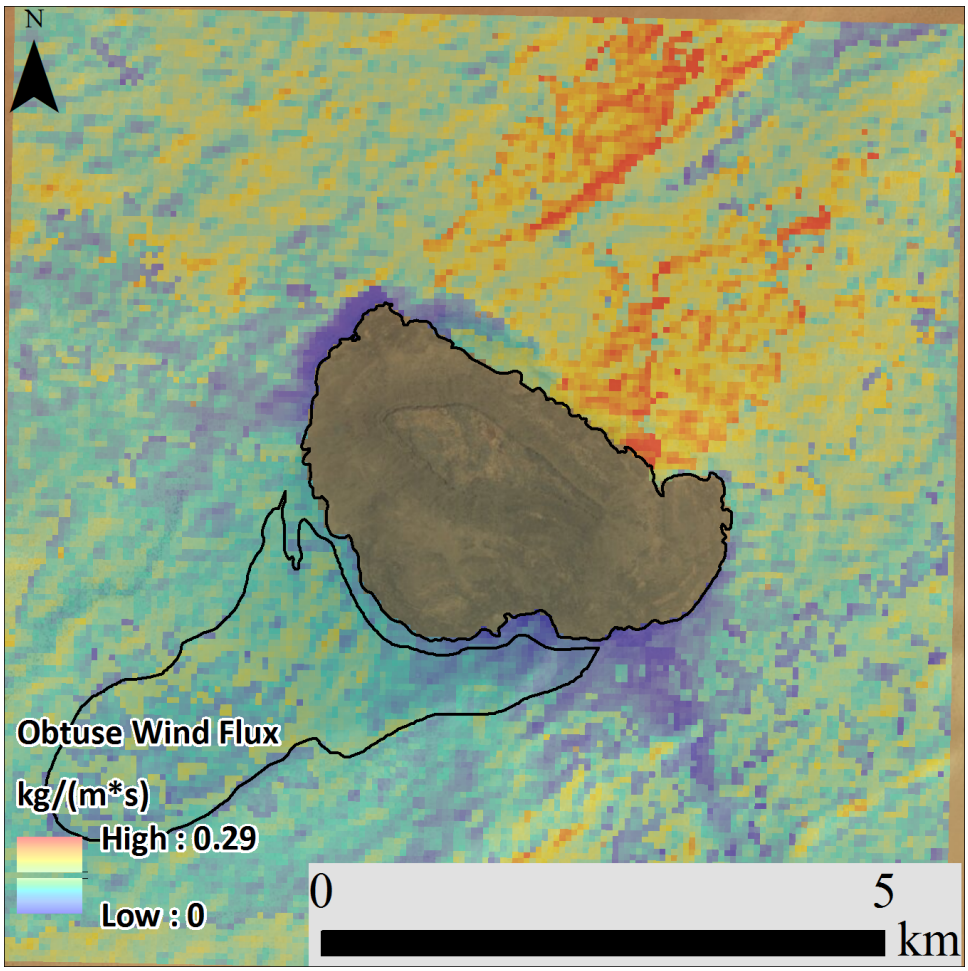

Figure 20: Estimated mass flux from an obtuse wind scenario - winds from 120º and 345º. Red corresponds to high flux and blue corresponds to low flux. The obstacle and lee-side basin are outlined in black.

Using the same modeled wind data, expected dune orientations were calculated and compared to the measured dune orientation (Figure 21). This revealed a low error between the predicted dunes from OpenFOAM and the mapped superimposed linear dunes in the lee side of the obstacle. The lowest error corresponds to dunes directly adjacent to the availability-limited lee-side basin. Further away from the basin, error increases, but the error is still relatively low in the lee side areas. It is noted that dunes directly adjacent to the obstacle have a high error in prediction, but the error decreases further away from the obstacle in the upwind side. About 500 m away from the obstacle on the upwind side, the error is similar to errors in the lee side of the obstacle.

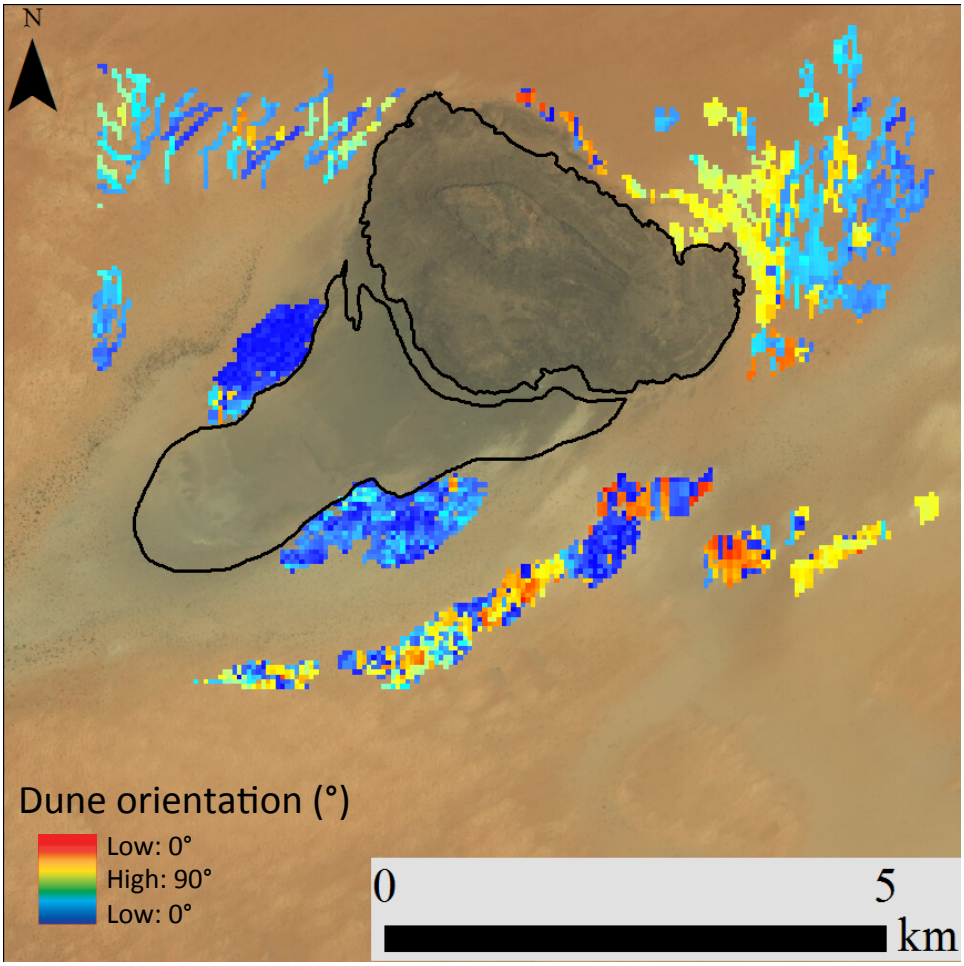

Figure 21: Dune orientation error between predicted and mapped dunes. In this image, blue and red correspond to low error, and yellow corresponds to high error. Error ranges from 0º-90º. The obstacle and lee-side basin are also outlined in black.

SECTION IV

DISCUSSION

7. Earth Geomorphic Mapping Discussion

Geomorphic mapping around the Earth obstacle reveals that it has a complex geomorphic surrounding environment. On Earth the obstacle has its own drainage system, including alluvial fans, and an availability-limited lee-side basin. Dunes vary in orientation and type in various areas around the obstacle. We hypothesize that the basin could be bedrock, a product of crusting, or could be wet or damp from a water table. We also note that the differing orientations of linear dunes could be due to secondary flow, or turbulence, around the obstacle. Secondary flow accounts for the deflected dunes around the obstacle in the upwind side. While the environment of the Earth obstacle is complex, we also see complexities in the environment around the Titan obstacle.

8. Titan Radar Unit Mapping Discussion

The radar units identified in the Titan study area include a topographic obstacle, obstacle adjacent radar mottled sheet, linear dunes, deflected dunes, and interdune areas (Figure 10). The obstacle here is the previously mentioned elliptical shaped radar bright area (Lorenz et al., 2006; Radebaugh et al., 2010). Adjacent to the obstacle is a mottled radar dark and bright area. This area is directly adjacent to the obstacle and in the inferred lee of the obstacle, but we do not have high enough resolutions to understand the varying degrees in brightness. Nevertheless, due to its location, we infer this area is similar to the availability-limited lee-side basin found on Earth. The next radar unit we identified is the radar dark streaks, which are interpreted as linear dunes (Lorenz et al., 2006; Radebaugh et al., 2010). We also denoted another radar unit as deflected

dunes, and these are linear dunes that at some point curve. The dune deflection happens very close to the obstacle, but dunes also encroach on top of or into the obstacle. This only happens on Titan. Interestingly, the dunes on Titan are all one size and type at the resolution of the radar, while the dunes on Earth are split into superimposed and larger, complex crescent dunes. Overall, dunes are not separated into populations around the obstacle, and they seem to be part of a larger dune field.

9. CFD Analysis Discussion

Through the WindNinja analysis, we see the predicted dunes do not match up with dunes in the lee side or dunes directly adjacent to the obstacle. This likely arises because WindNinja does not capture the secondary flow (turbulence) that affects the dune orientation in the obstacle lee and directly adjacent to the obstacle. We also think that the dune orientation in the lee depends on sediment availability, or lack thereof, in the lee side (Courrech du Pont et al., 2014). We infer that the alignment of dunes on the upwind side of the obstacle reflects the regional winds and recent dune orientation. Moreover, the predicted dunes on Titan do not match up with the mapped dunes. We believe this could be due to several reasons including: the wind from the GCM is too generalized for this obstacle area, WindNinja does not capture secondary flow, and the topographic data swath needs further processing. As of now, we believe the topographic data, as it is, is scaled too small for WindNinja to accurately modify winds around an obstacle.

From the OpenFOAM analysis we see the topographic shape of the obstacle exerts a strong influence on the spatial distribution of the wind. This is most noticeable in the difference between a modeled wind from 044º and from 060º. Although these winds only differ by 16º, the

spatial distribution of the winds is dramatically different, most significantly seen by the offset of the tail. Results from the summed fluxes show the unimodal and acute winds have low flux in the lee and higher flux along the sides of the obstacle. This means that in the lee there is a small amount of sediment being moved and along the sides there is a large amount of sediment being moved. Conversely, the obtuse winds have a low flux along the sides of the obstacle and a higher flux in the lee. This means that sediment is not being moved along the sides of the obstacle, but there is sediment being moved in the lee of the obstacle. The obtuse scenario tells us that obtuse winds that could form longitudinal linear dunes could also transport sediment into the lee of the obstacle. This is different from what we expect from unimodal and acute winds and from what we see in this availability-limited lee-side basin.

Finally, the dune error analysis between mapped and predicted dunes tells us about how well OpenFOAM is predicting dunes around the Earth obstacle. The error is low in the lee and further away from the obstacle, but the error is high directly adjacent to the obstacle (Figure 21). This means that OpenFOAM is predicting dune orientations very well in the lee and further away from the obstacle, but is predicting dune orientations poorly directly adjacent to the obstacle. From this, we can say that OpenFOAM is modeling the secondary flow in the lee of the obstacle accurately, but it may not be modeling the secondary flow that happens when the wind meets the base of the obstacle in the upwind side.

REFERENCES

Courrech du Pont, S., Narteau, C., Gao, X., 2014. Two modes for dune orientation. Geology 42, 743–746. doi:10.1130/G35657.1

Eastwood, E.N., Kocurek, G., Mohrig, D., Swanson, T., 2012. Methodology for reconstructing wind direction, wind speed and duration of wind events from aeolian cross-strata. J. Geophys. Res. 117, F03035. doi:10.1029/2012JF002368

Ewing, R.C., Hayes, A.G., Lucas, A., 2015. Sand dune patterns on Titan controlled by long-term climate cycles. Nat. Geosci. 8, 15–19. doi:10.1038/ngeo2323

Ewing, R.C., Kocurek, G., Lake, L.W., 2006. Pattern analysis of dune-field parameters. Earth Surf. Process. Landforms 31, 1176–1191. doi:10.1002/esp.1312

Forthofer, J.M., 2007. MODELING WIND IN COMPLEX TERRAIN FOR USE IN FIRE SPREAD PREDICTION. Color. State Univ. Thesis.

Livingstone, I., 2003. A twenty-one-year record of surface change on a Namib linear dune. Earth Surf. Process. Landforms 28, 1025–1031. doi:10.1002/esp.1000

Lorenz, R.D., Wall, S., Radebaugh, J., Boubin, G., Reffet, E., Janssen, M., Stofan, E., Lopes, R., Kirk, R., Elachi, C., Lunine, J., Mitchell, K., Paganelli, F., Soderblom, L., Wood, C., Wye, L., Zebker, H., Anderson, Y., Ostro, S., Allison, M., Boehmer, R., Callahan, P., Encrenaz, P., Ori, G.G., Francescetti, G., Gim, Y., Hamilton, G., Hensley, S., Johnson, W., Kelleher, K., Muhleman, D., Picardi, G., Posa, F., Roth, L., Seu, R., Shaffer, S., Stiles, B., Vetrella, S., Flamini, E., West, R., 2006. The sand seas of Titan: Cassini RADAR observations of longitudinal dunes. Science 312, 724–7. doi:10.1126/science.1123257

Lucas, A., Aharonson, O., Deledalle, C., Hayes, A.G., Kirk, R., Howington-kraus, E., Al, L.E.T., 2014a. Insights into Titan ' s geology and hydrology based on enhanced image processing of Cassini RADAR data 2149–2166. doi:10.1002/2013JE004584.Received

Lucas, A., Rodriguez, S., Narteau, C., Charnay, B., Courrech du Pont, S., Tokano, T., Garcia, A., Thiriet, M., Hayes, A.G., Lorenz, R.D., Aharonson, O., 2014b. Growth mechanisms and dune orientation on Titan. Geophys. Res. Lett. n/a–n/a. doi:10.1002/2014GL060971

Radebaugh, J., Lorenz, R., Farr, T., Paillou, P., Savage, C., Spencer, C., 2010. Linear dunes on Titan and earth: Initial remote sensing comparisons. Geomorphology 121, 122–132. doi:10.1016/j.geomorph.2009.02.022

Rubin, D., Hunter, R., 1987. Bedform alignment in directionally varying flows. Science (80-.).

Rubin, D.M., Hesp, P.A., 2009. Multiple origins of linear dunes on Earth and Titan. Nat. Geosci. 2, 653–658. doi:10.1038/ngeo610

Smyth, T. a. G., Jackson, D.W.T., Cooper, J.A.G., 2012. High resolution measured and modelled three-dimensional airflow over a coastal bowl blowout. Geomorphology 177-178, 62–73. doi:10.1016/j.geomorph.2012.07.014

Tokano, T., 2010. Relevance of fast westerlies at equinox for the eastward elongation of Titan's dunes. Aeolian Res. 2, 113–127. doi:10.1016/j.aeolia.2010.04.003

APPENDIX

Appendix A: Matlab Code of Loop from WindNinja to GBNT function

```
%   A script to get wind vectors from WindNinja representing interactions with topography.

%   After getting modified wind vectors, it runs the winds through the

%   GBNT.

%   The final output is a spatial orientation matrix.

%   Outputs are found in the DEM file location folder.

%   Resolution is matched to the resolution of the DEM.

%   Written by Julia Cisneros, Texas A&M University. July 2014


%INPUTS: DEM file location

%       The threshold you would like to use

%       .csv file location  that includes 2 columns: wind speed and wind direction, respectively.

%      This is meant to be easier to use, so all you have to do is type in the inputs when the script
       asks for it.


%NOTE:

%    Be sure you add the path from which you will be working (using addpath(genpath()) ). So
     change this

%    file directory to the file you are working from. THIS MUST INCLUDE THE DEM

%    AND THE GBNT FUNCTION. you will be pulling the GBNT function at the end of

%    this script.


dem = input('DEM file location: ')   %load DEM (digital elevation) file -- as a string
```

```
thresh = input('Desired threshold: ')    %input desired threshold for wind -- as a string


%   Load the wind vectors from a mat file

wind = input('csv file of wind vectors: ')  %load the csv that includes the winds you will be
       running through windninja

load(wind)

speed= wind(:,1);

direction= wind(:,2);   %make sure all directions are greater than 0


 N=length(direction);          %find number of rows in file


for i=1:N

    spd = num2str(speed(i));

    spd = strcat(' ',spd);          %adding a space before spd

    az = num2str(direction(i));

    az = strcat(' ',az);         %adding a space before az

    % here we are calling the command line to open windninja and run one

    % wind.

    exec_path = 'WindNinja_cli.exe D:\Julia\Topographicobstacles\cli_General_Earth.cli --
       input_speed ';  %you will have to change the file directory of the .cli file within this text to
       where it is located in your folders.


    str = horzcat(exec_path, spd, ' --input_direction ', az, ' --elevation_file ', dem);

    [x,y] = system(str);                %[x,y] is used to suppress the system output (running
       WindNinja)
```

```
name = dir ('*ang.asc') ;              %store direction data in a matrix and concatenate them in the
   3rd dimension

name = name.name;

temp_data = importdata(name,'\t',6);

temp_data = temp_data.data;


%create the output vectors if they don't exist

if ~exist('dir_vec','var');

   dir_vec = zeros(size(temp_data,1),size(temp_data,2),N);

   spd_vec = dir_vec;

end;


dir_vec(:,:,i) = temp_data;


name1 = dir ('*vel.asc') ;             %store speed data in a matrix and concatenate them in the
   3rd dimension

name1 = name1.name;

temp_data1 = importdata(name1,'\t',6);

temp_data1 = temp_data1.data;


spd_vec(:,:,i) = temp_data1;


u=-spd_vec.*sind(dir_vec);      %this sets u and v vectors for the wind. u and v vectors are
   easier to work with and are needed for the GBNT
```

```
    v=-spd_vec.*cosd(dir_vec);



    prevState = recycle('off'); % turn recycle off to permanently delete files
    delete('*.asc','*.prj');     % deleting the files
    recycle(prevState);          % restore the state of recycle

% so now we saved the wind data (speed and direction) to files that have
% _vel.asc and _ang.asc file extensions. We keep turning of windninja and
% re running it, saving winds to these files, over and over until all the
% winds have been run through windninja.
end



        % save matrices in .mat file (wind_vec.m)
file=('wind_vec.mat');



%Squeeze u and v to only look at one location vs. time
for i=1:size(u,1); for j= 1:size(u,2);
        [orientation(i,j)]=GBNT(squeeze(u(i,j,:)),squeeze(v(i,j,:)),[],thresh);
    end; if mod(i,10) == 0; disp(i); end; end; %this will count how many winds you have run
       through, so you can tell where you are in this step.


save(file, 'spd_vec', 'dir_vec', 'u', 'v', 'orientation');
```